MEDDOCS Open Access Publisher

Nanoscience and Nanotechnology: Open Access

Open Access | Research Article

Biosynthesis and Characterization of $CuO\text{-}CuMn_2O_4$ Nano Particles for Biomedical Applications

Mai Nasrallah[1]; Mohamed Nasrallah[2]*

[1]Faculty of Medicine, Ain Shams University, El-Khalyfa El-Mamoun Street, Abbasya, Cairo, Egypt.

[2]Faculty of Medicine, Ibn Sina University, Aljerif west block (88), Khartoum, Sudan.

Corresponding Author(s): Mohamed Nasrallah

Faculty of Medicine, Ibn Sina University, Aljerif west block (88), Khartoum, Sudan.
Email: nm.mahmoud@nrc.sci.eg

Received: Aug 18, 2023

Accepted: Sep 12, 2023

Published Online: Sep 18, 2023

Journal: Nanoscience and Nanotechnology: Open Access

Publisher: MedDocs Publishers LLC

Online edition: http://meddocsonline.org/

Keywords: $CuO\text{-}CuMn_2O_4$ NPs; XRD; SEM; EDX; VSM.

Abstract

This study focused on preparation of copper oxide -copper manganite nanoparticles ($CuO\text{-}CuMn_2O_4$ NPs) via new method. This method is based on replacement of the traditional routes by egg white assisted green synthesis. In other words, the goal of this investigation is preparation of composite containing $CuO\text{-}CuMn_2O_4$ NPs by using a facile one-step method. The as synthesized material was characterized using X-Ray Diffraction (XRD), Energy-Dispersive X-Ray spectroscopy (EDX), Scanning Electron Microscope (SEM). The magnetic properties of the prepared sample have been measured by using a Vibrating Sample Magnetometer (VSM). XRD, EDX and SEM resulted in a successful synthesis of $CuO\text{-}CuMn_2O_4$ system with sponge crystal structure. The particles of the prepared composite are polycrystalline in their nature and average sizes ranged between 40 and 90nm. The magnetic measurement indicated that the obtained nanostructured materials is found to show room temperature ferromagnetism with an optimum value (0.818emu/g) of saturation magnetization.

Introduction

The properties of nano sized materials are strongly related to the preparation processes. In other words, the synthetic processes are the key step and starting point for obtaining specific properties of the material [1-3]. However, many benefits of nanotechnology depend on the fact that it is possible to tailor the structures of materials at extremely small scales to achieve specific properties, thus greatly extending the materials science toolkit. So, the preparation techniques of the materials are the rate determining steps for nanotechnology. Indeed, nanotechnology is helping to considerably improve, even revolutionize, many technology and industry sectors such as information technology, homeland security, medicine, transportation, energy, food safety, and environmental science. Thus, preparation and applications of nanosized materials are significant scientific and industrial interests due to their unique or improved properties, which are primarily determined by size, composition and structure [4-6]. Use of nanoparticles have established benefits in a wide range of applications, however, the effects of exposure to nanoparticles on health and the environmental risks associated with the production and use of nanoparticles are less well-established. In other words, nanoparticles offer distinct benefits in a range of applications, they pose significant threats to humans and the environment. Using several biological models and biomarkers, the included studies revealed the toxic effects of nanoparticles (mainly zinc oxide, silicon dioxide, titanium dioxide, silver, and carbon nanotubes) to include cell death, production of oxidative stress, DNA damage, apoptosis, and induction of inflammatory responses [7].

Cite this article: Nasrallah M, Nasrallah M. Biosynthesis and Characterization of $CuO\text{-}CuMn_2O_4$ Nano Particles for Biomedical Applications. Nanosci Nanotechnol Open Access. 2023; 2(2): 1015.

Copper oxide (CuO) is an important industrial material with different properties such as electrical, optical and catalytic properties. CuO has many applications like magnetic ceramics, gas sensors, electrode materials, solar cells, hydrogen storage materials and photocatalysis [8,9]. Spinel oxides AB_2O_4 have attracted since long time scientific and technological interest resulting in many important applications ranging from electronics, optics, magnetism, catalysis to energy storage and conversion. Manganite spinels AMn_2O_4 represent such multifunctional materials in which adjusting the quantity and the chemical identity of A^{2+} permits to reach a wide range of properties. The copper manganite $Cu_xMn_{3-x}O_4$ "Hopcalites", being an example of such a system presents a distinguished feature of having a flexible valence in $Cu^{1+/2+}$ and $Mn^{3+/4+}$ giving rise to its particular properties [10,11].

Hopcalite is still a catalyst of choice in respiratory protection for many applications including military, scubadiving, fire fighting, mining and space. Cu-Mn oxide catalysts have been shown also efficient in reactions such as water-gas shift, NO reduction with CO, direct NO decomposition, selective oxidation of ammonia to N_2 and more recently in the catalytic steam reforming of methanol, oxidative methanol reforming, preferential CO oxidation as well as in selective oxidation of toluene to benzoic acid and benzyl alcohol to benzaldehyde [12-14].

Conventionally the Cu-Mn-O systems are prepared by either coprecipitation or high temperature ceramic method [15,16]. In recent years, alternative preparation methods were used for production Cu-Mn solids such as sol-gel, redox-precipitation, soft reactive grinding, synthesis under supercritical water conditions, reverse microemulsion, and the combustion method [17-24]. These routes resulted in enhancement of textural properties for the as synthesized solids with taken into account the environmental impact of the material precursor [25].

In this paper we demonstrate for the first time experimental method for the preparation of nanosized CuO - $CuMn_2O_4$ composite by using egg white as bio material auxiliary providing nanoscale oxide dispersion in one step. The single-step process is facile, environment-benign, inexpensive, and reproducible, yielding high-quality CuO - $CuMn_2O_4$ nanocomposite that can be controlled in terms of structure, morphology, size, and size distribution. Characterization of the produced NPs and magnetic properties were determined.

Experimental

Preparation of nanocomposite

One sample of CuO - $CuMn_2O_4$ nanocomposite was prepared. The starting point of the synthesis procedure was the formation of an egg white–based precursor from copper nitrate trihydrate and manganese nitrate tetrahydrate. The reagents were diluted in water taking into account the stoichiometric ratio Mn/Cu = 2. Egg white (2.5ml) was added into the mixture until a transparent sol was obtained. The obtained mixture was stirred first at 60 °C to evaporate water and increase the viscosity. Then the solution was heated at 120 °C, to create a gel. The resulting precursor gel was calcined in a furnace at 300 °C for 15min. When a crucible temperature was reached, great deal of foams produced and spark appeared at one corner which spread through the mass, yielding a voluminous and fluffy product in the container. A black powder was obtained as final product. The chemicals employed in the present work were of analytical grade supplied by Prolabo Company. A general flowchart of the synthesis process is shown in Figure 1.

Characterization techniques

An X-ray measurement of various mixed solids was carried out using a BRUKER D8 advance diffractometer (Germany). The patterns were run with Cu K_α radiation at 40 kV and 40 mA with scanning speed in 2q of 2 ° min^{-1}.

The crystallite size of CuO and $CuMn_2O_4$ present in the investigated solids was based on X-ray diffraction line broadening and calculated by using Scherrer equation [26].

$$d = \frac{B\lambda}{\beta \cos\theta} \qquad (1)$$

where d is the average crystallite size of the phase under investigation, B is the Scherrer constant (0.89), λ is the wave length of X-ray beam used, β is the full-width half maximum (FWHM) of diffraction and θ is the Bragg's angle.

Scanning Electron Micrographs (SEM) was recorded on JEOL JAX-840A electron micro-analyzer. The samples were dispersed in ethanol and then treated ultrasonically in order to disperse individual particles over gold grids.

Energy Dispersive X-Ray analysis (EDX) was carried out on JEOL (JED- 2200 Series) electron microscope with an attached kevex Delta system. The parameters were as follows: accelerating voltage 15 kV, accumulation time 100s, window width 8 µm. The surface molar composition was determined by the Asa method, Zaf-correction, Gaussian approximation.

Vibrating sample magnetometer (VSM; 9600-1 LDJ, USA) used to investigate the magnetic properties of the investigated solids in a maximum applied field of 15 kOe. Hysteresis loops, saturation magnetization (M_s), remanence magnetization (M_r) and coercivity (H_c) were determined.

Results

XRD investigation

The XRD pattern of the as synthesized nanocomposite containing both CuO and $CuMn_2O_4$ NPs is illustrated in Figure 2. The XRD pattern showed a series of diffraction peaks at degree 2ϑ = 35.61, 37.51, 53.98, 57.25, and 63.40 characteristic to indexing planes (311), (222), (400), (511) and (440), respectively. This agrees with the values reported for spinel $CuMn_2O_4$ NPs (JCPD file No. 74-1919). However, this pattern showed another series of diffraction peaks at degree 2ϑ = 35.44, 38.69, 49.93, 52.99, 58.40 and 65.56 characteristic to indexing planes (002, 111), (111, 200), (202), (020), (202) and (022), respectively. This agrees with the values reported for CuO NPs (JCPD file No. 72-0629). The mean crystallite size of the CuMn2O4 and CuO particles were calculated depending upon Scherer's formula [26]. The values of the crystallite size (d), X-ray density (D_x), unit cell volume (V), lattice constant (a), dislocation density (ρ_d) and micro-strain (ε) of the as synthesized composite are shown in Table 1.

Energy Dispersive X-Ray (EDX) Analysis

Figure 3 displays the EDX pattern of the as synthesized nanocomposite. It was observed from this figure presence of the signal characteristic of copper (Ni), manganese (Mn) and oxygen (O) elements. In addition, the weights percent of Cu, Mn and O calculated from EDX were 11.30 wt%, 66.49 wt% and 22.21 wt %, respectively. No signals arising from any impurity have been

detected in the EDX spectrum. These findings confirm the presence of both CuO- $CuMn_2O_4$ nanocomposite.

Scanning Electron Microscopic (SEM) Analysis

The surface morphology of the synthesized Cu-Mn mixed oxides was investigated using SEM analysis. The SEM images with different magnifications were collected in Fig. 4. Figure 4 from 4a to 4e represents the SEM images of CuO-$CuMn_2O_4$ solid obtained by using egg white assisted green synthesis. From the SEM images of this composite, it was observed that the particles have spongy structure containing pores and voids. However, these particles have a higher tendency of agglomerations. The synthesized nanoparticles had sizes ranged between 40 and 90nm indicating formation of polycrystalline solid. These observations confirm that the prepared CuO-$CuMn_2O_4$ particles are unhomogeneity and also are in agreement with XRD measurement.

Magnetic study

The magnetic characteristics of the CuO-$CuMn_2O_4$ NPs were measured at room temperature by a vibrating sample magnetometer (VSM). The plots of magnetization (M) as a function of applied magnetic field (H) are shown in Fig. 5. This figure shows hysteresis cycle measured at 300 K. Table 2 contains the values of the saturation magnetization (M_s), remenant magnetization (M_r), the squareness or the ratio of remenant magnetization to saturation magnetization (M_r/M_s), coercive force or coercivity (H_c) and anisotropy constant (K_a) for the as synthesized composite. These results agree with many reports [27,28].

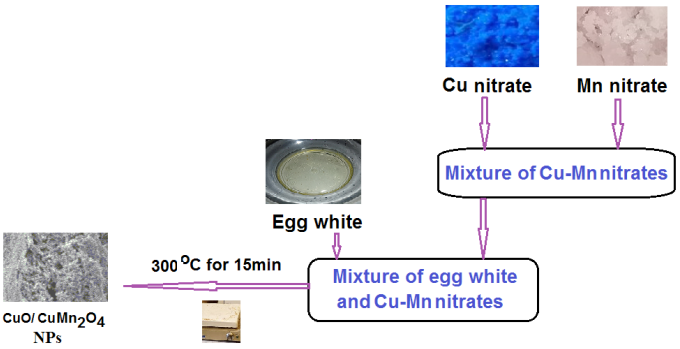

Figure 1: Experimental flow chart for the synthesis of CuO-CuMn2O4 nanocomposite by egg white assisted green method.

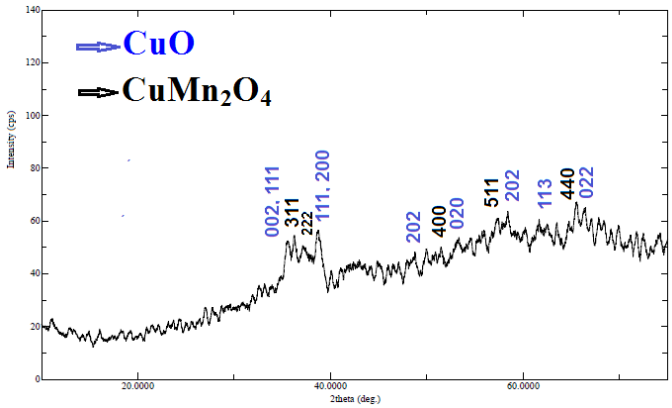

Figure 2: XRD pattern of CuO-CuMn2O4 nanocomposite.

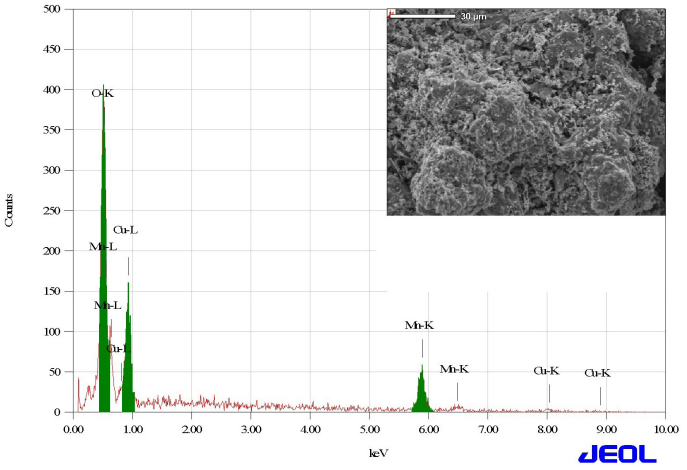

Figure 3: EDX pattern of CuO-CuMn2O4 nanocomposite.

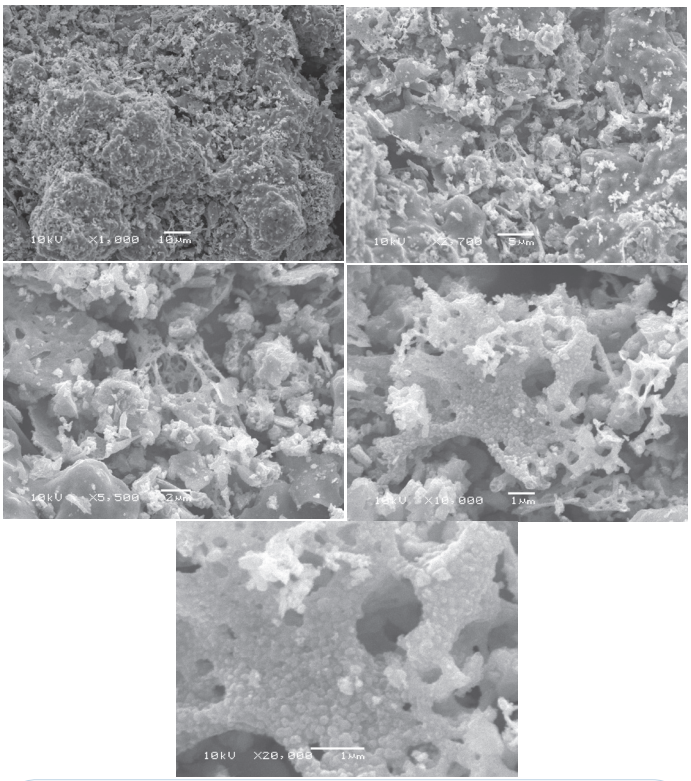

Figure 4: (a-e). SEM images of CuO-CuMn2O4 nanocomposite with different magnifications.

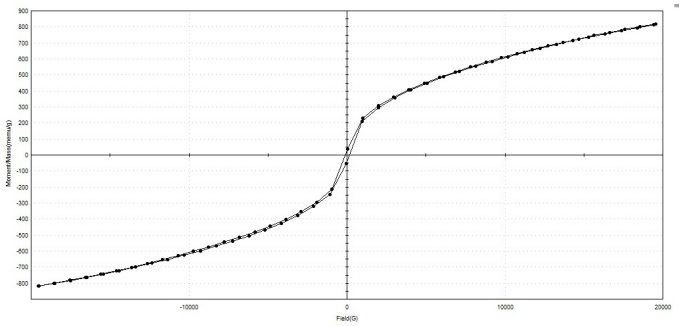

Figure 5: M-H curve for CuO-CuMn2O4 nanocomposite.

Table 1: Some structural properties of CuO and CuMn2O4 NPs Involved in the prepared nanocomposite.

Properties	Values	
	CuO	$CuMn_2O_4$
Crystal structure	Monoclinic	Cubic spinel
Lattice constant, nm	a= 0.4672 b= 0.3108 c= 0.5125	a=b=c=0.8355
Unit cell volume (V), nm^3	0.0809	0.5832
Density (D_x), g/cm^3	6.455	5.4030
Dislocation density (ρ_d)	$1.78x10^{-4}$	$4.94 x10^{-4}$
Crystallite size (d), nm	75	45
Micro-strain (ε)	0.1196	0.1197

Table 2: Magnetic properties of the as synthesized nanocomposite.

Properties	Values
Saturation magnetization (M_s) emu/g	0.8179
Remenant magnetization (M_r) emu/g	$32.359x10^{-3}$
Coercivity (H_c)Oe	126.53
Squareness (M_r/M_s)	$39.559x10^{-3}$
Anisotropy constant (K_a)	105.60

Discussion

In this investigation, the egg white mediated green synthesis brought about formation of CuO-$CuMn_2O_4$ nanocomposite with mean average crystallite was approximately 60nm. Indeed, the broadened peaks in the XRD pattern of the as prepared solid confirm that the crystal size of this solid is small. However, it can be seen from Table 1 that there is micro-strain and dislocation in the crystal lattice of CuO and $CuMn_2O_4$ nanoparticles. A dislocation is a crystallographic defect (irregularity) within a crystal structure, which strongly influences the properties of materials. This defect distorts the regular atomic array of a perfect crystal [29-31]. The strain confirms presence of defects inside the crystal lattices.

In addition, copper manganite can be prepared by ceramic route via solid state reaction between Cu and Mn oxides [21,24]. The rate determining step in the propagation of this reaction is the thermal diffusion of Cu and Mn cations through the thin manganite film which covers the surfaces of grains of reacting Cu and Mn oxides. This film acts as energy barrier to prevent the formation of excess amounts of manganite. But, the promotion of this diffusion can be achieved by techniques such as doping, heat treatment, prolonged time of heat treatment and preparation route [21,24]. The formation of copper manganite is according to the following stoichiometric reaction:

$$CuO + Mn_2O_3 \rightarrow CuMn_2O_4 \quad (2)$$

Copper manganite crystallizes in an inverse cubic spinel structure where manganese ions are distributed among the tetrahedral and octahedral sites [24]. In fact, the presence of the Mn^{n+1}/Mn^{n+} redox couple located in B-sites of the semiconductor spinel has been considered as the responsible factor of the controlled-valence conduction mechanism proposed by Verwey [32]. Moreover, Cu^+ ions have a strong preference for tetrahedral interstices [33-35]. In addition, Mn^{3+} ions in octahedral sites disproportionate to Mn^{2+} and Mn^{4+}, then Mn^{2+} ions will move to tetrahedral sites [36,37]. On the other hand, the counter-diffusion of copper and manganese ions through a relatively rigid manganite film led to the formation of $CuMn_2O_4$ particles. Moreover, oxygen moves through the reacted area to be added to the CuO interface and form spinel by reacting with manganese ions. Consequently, we see that the proposed mechanism of formation of $CuMn_2O_4$ NPs is as following:

At Mn_2O_3 interface:

$$3Mn_2O_3 + 2\,Cu^{2+} \rightarrow 2CuMn_2O_4 + Mn^{2+} + Mn^{4+} + 0.5O_2 \quad (3)$$

At CuO interface:

$$3CuO + Mn^{2+} + Mn^{4+} + 0.5O_2 \rightarrow CuMn_2O_4 + 2\,Cu^{2+} \quad (4)$$

It was later reported that pure cubic spinel $CuMn_2O_4$ could not be prepared at all [33-35]. Several authors reported that Cu^+ can be formed during the sintering process of Cu-containing spinel materials. However, any oxidation of Cu^+ to Cu^{2+} on cooling in air does not cause an incorporation of the residual CuO into the spinel phase [24,38]. Similar results were observed in our previous works which indicate to formation of $CuMn_2O_4$ with Mn_2O_3 by using ceramic method via the thermal treatment of equimolar ratio of copper chloride and manganese carbonate [24]. The comparison between this study and our previous works confirms the role of metal precursor and preparation method in change of the crystallographic of product.

SEM results confirmed the nano regime range of the synthesized CuO-$CuMn_2O_4$ nanocomposite with high agglomeration. It was evident from the EDX spectrum that the CuO-$CuMn_2O_4$ nanocomposite was synthesized successfully depending upon the major constituents of the as prepared sample were Cu, Mn and O elements without any impurities. However, results of EDX of the as synthesized solid were consistent with that of XRD. However, the higher particle size of the prepared composite could be attributed to presence of Cu^+ ions with higher ionic radius (0.96nm) involved in spinel structure [33-35].

The biosynthesized CuO-$CuMn_2O_4$ nanocomposite exhibit magnetic hysteresis loops with coercivity (126.53Oe) and saturation magnetization (0.8179emu/g). In order to understand the mechanism responsible for ferromagnetism in CuO-$CuMn_2O_4$ nanocomposite, the origin of ferromagnetism is analyzed by different possibilities that can be present in this system. In other words, CuO-$CuMn_2O_4$ nanocomposite has a ferromagnetic-like state depending upon the competition between ferromagnetic and antiferromagnetic sublattices [38,39]. This competition could be attributed to the presence of a complex magnetic structure with existence of several magnetic sublattices in the oxides. Some authors were observed the Mn^{2+}- Mn^{3+} antiferromagnetic interactions at low temperatures [40]. These authors reported to Mn^{3+} and Mn^{4+} ferromagnetic interactions at higher temperature close to the magnetic transition. The interaction between Cu^{2+} and Mn^{3+} ions has been suggested to be ferromagnetic [38, 39]. It is reasonable to believe that the indirect coupling between Mn ions mediated by O and Cu ions helps to stabilize the ferromagnetism [41]. Additionally, Cu-O-Cu interactions may also play a role.

Conclusion

For the first time, egg white assisted green synthesis resulted in formation of CuO-$CuMn_2O_4$ nanocomposite. This method has many advantages such as non toxic, economic viability, ease to scale up, less time consuming and environmental friendly ap-

proach for the synthesis of CuO-$CuMn_2O_4$ nanocomposite without using any additives. From XRD results, the as synthesized material consisted entirely of CuO-$CuMn_2O_4$ nanocomposite. The elements and morphology of the prepared sample were characterized using EDX and SEM techniques. In future, this green method of synthesizing CuO-$CuMn_2O_4$ nanocomposite could also be extended to the fabrication of other industrially important composites.

References

1. NM Deraz. J. Ind Environ Chem. 2018; 2: 16-18.
2. NM Deraz. J. Ind Environ Chem. 2018; 2: 19-21.
3. NM Deraz. J. Ind Environ Chem. 2018; 2: 1-3.
4. KC Kwiat Kowski, CM Lukehar. Handbook of nano structured materials and Nano technology. HS. Nalwa, eds. Academic Press. 2000.
5. I Brigger, C Dubernet, P Couvreur. Adv. Drug. Delive. Rev. 2002; 54: 631.
6. I Safarik, M Safarikova. Mate. R Sci. Eng. 2002; 133: 737.
7. EA Kumah, RD Fopa, S Harati, P Boadu, FV Zohoori, et al. BMC Public Health. 2023; 23: 1059.
8. P Gao, Y Chen, H Lu, X Li, Y Wang, et al. Int. J. Hydrogen Ener. 2009; 34: 3784.
9. M Yao, Y Tang, L Zhang, H Yang, J Yan. Trans. Nonferrous Met. Soc. China. 2010; 20: 1944.
10. DR Merrill, CC Scalione. Journal of the American Chemical Society. 1921; 43: 1982.
11. JS Rowlinson, Notes and Records of the Royal Society of London. 2004; 58: 161.
12. Kd Zhi, Qs Liu, Yg Zhang, S He, Rx He. Journal of Fuel Chemistry and Technology. 2010; 38: 445.
13. Q Liu, LC Wang, M Chen, YM Liu, Y Cao, et al. Catalysis Letters. 2008; 121: 144.
14. T Valdes-Solis, I Lopez, G Marban. International Journal of Hydrogen Energy. 2010; 35: 1879.
15. Q Tang, X Gong, P Zhao, Y Chen, Y Yang. Applied Catalysis A: General. 2010; 389: 101.
16. GJ Hutchings, AA Mirzaei, RW Joyner, MRH Siddiqui, SH Taylor. Applied Catalysis A: General. 1998; 166: 143.
17. M Zimowska, A Michalik-Zym, R Janik, T Machej, J Gurgul, et al. Catalysis Today. 2007; 119: 321.
18. WB Li, WB Chu, M Zhuang, J Hua. Catalysis Today. 2004; 205: 93-95.
19. M Kramer, T Schmidt, K Stowe, WF Maier. Applied Catalysis A: General. 2006; 302: 257.
20. VH Vu, E Ndzebet, A Kumar, D Gilbert, WC Bushong, et al. Copper-manganese mixed oxide cathode material for use in alkaline cells having high capacity, US Patent to Roval Inc., Madison, WI, United States. 2010; 7: 296.
21. D Rangappa, S Ohara, M Umetsu, T Naka, T Adschiri. The Journal of Supercritical Fluids. 2008; 44: 441.
22. NM Deraz, Ahmed A Abdeltawab, MM Selim, O El-Shafey, AA El-Asmy, et al. Journal of Industrial and Engineering Chemistry. 2014; 20: 2901- 2904.
23. NM Deraz, Omar H Abd-Elkader. Asian Journal of Chemistry. 2014; 26: 2125-2128.
24. NM Deraz, Omar H Abd-Elkader. Asian Journal of Chemistry. 2014; 26: 2133-2137.
25. SA Kondrat, TE Davies, ZL Zu, P Boldrin, JK Bartley, et al. Journal of Catalysis. 2011; 281: 279.
26. BD Cullity. Elements of X-ray Diffraction, Addison-Wesly Publishing Co. Inc. 1976; 14.
27. F Afriani, Ciswandi, B Hermanto, T Udiro. Synthesis of CuMn2O4 spinel and its magnetic properties characterization, Proceedings of the International Seminar on Metallurgy and Materials (ISMM2017) AIP Conf. Proc. 1964; 020016-1-020016-6.
28. Shahzad Hussain, A Mumtaz, SK Hasanain, M Usman, J Appl. Phys. 2012; 111: 023908.
29. MK Rendale, SN Mathad, V Puri. Int. J. Self-Propag. High-Temp. Synth. 2015; 24: 112.
30. SN Mathad, RN Jadhav, ND Patil, V Puri. Int. J. Self-Propag. High-Temp. Synth. 2013; 22: 180.
31. SN Mathad, RN Jadhav, V Phadatare, V Puri, Int. J. Self-Propag. High-Temp. Synth. 2014; 23: 145.
32. EJW Verwey. Oxidic Semiconductors in Semi-conducting Materials. H.K. Henisch (Ed) London Butterworths Sc Pub Ltd. 1951; 151.
33. G Blasse. J. Phys. Chem. Solids. 1966; 27: 383.
34. R Buhl. J. Phys. Chem. Solids. 1969; 30: 805.
35. GG Robbrecht, CM Henriet-Iserentant, Phys. Status Solidi. 1970; 41: K43.
36. HR Jung, SG Lee, DJ Lee, KM Kim. Journal of Ceramic Processing Research. 2016; 17: 758.
37. A Bielanski, K Dyrek, Z Kluz, J Slozynski, T Tombiasz. Bull. Acad. Pol. Sci. 1964; 9: 657.
38. SG Yang, T Li, BX Gu, YW Du. Appl. Phys. Lett. 2003; 83: 3746.
39. XY Cue, JE Medvedeva, B Delley, AJ Freeman, N Newman, et al. Phys. Rev. Lett. 2005; 95: 256404.
40. PN Lisboa-Filho, M Bahout, P Barahona, C Moure, O Peña. J. Phys. Chem. Solids. 2005; 66: 1296.
41. H Zhu, F Zhao, L Pan, Y Zhang, C Fan, et al. J. Appl. Phys. 2007; 101: 09H111.